International Journal of Greenhouse Gas Control 3 (2009) 600–611

Contents lists available at ScienceDirect

International Journal of Greenhouse Gas Control

journal homepage: www.elsevier.com/locate/ijggc

Analytical solution to evaluate salt precipitation during CO_2 injection in saline aquifers

Mehdi Zeidouni *, Mehran Pooladi-Darvish, David Keith

Energy and Environmental Systems Group, Institute for Sustainable Energy, Environment, and Economy, University of Calgary, 2500 University Drive, Calgary AB, T2N 1N4, Canada

ARTICLE INFO

Article history:
Received 2 March 2008
Received in revised form 14 April 2009
Accepted 18 April 2009
Available online 22 May 2009

Keywords:
CO_2 sequestration
Salt precipitation
Analytical solution

ABSTRACT

Carbon dioxide sequestration in deep saline aquifers is a means of reducing anthropogenic atmospheric emissions of CO_2. Among various mechanisms, CO_2 can be trapped in saline aquifers by dissolution in the formation water. Vaporization of water occurs along with the dissolution of CO_2. Vaporization can cause salt precipitation, which reduces porosity and impairs permeability of the reservoir in the vicinity of the wellbore, and can lead to reduction in injectivity. The amount of salt precipitation and the region in which it occurs may be important in CO_2 storage operations if salt precipitation significantly reduces injectivity. Here we develop an analytical model, as a simple and efficient tool to predict the amount of salt precipitation over time and space. This model is particularly useful at high injection velocities, when viscous forces dominate.

First, we develop a model which treats the vaporization of water and dissolution of CO_2 in radial geometry. Next, the model is used to predict salt precipitation. The combined model is then extended to evaluate the effect of salt precipitation on permeability in terms of a time-dependent skin factor. Finally, the analytical model is corroborated by application to a specific problem with an available numerical solution, where a close agreement between the solutions is observed. We use the results to examine the effect of assumptions and approximations made in the development of the analytical solution. For cases studied, salt saturation was a few percent. The loss in injectivity depends on the degree of reduction of formation permeability with increased salt saturation. For permeability-reduction models considered in this work, the loss in injectivity was not severe. However, one limitation of the model is that it neglects capillary and gravity forces, and these forces might increase salt precipitation at the bottom of formation particularly when injection rate is low.

© 2009 Elsevier Ltd. All rights reserved.

1. Introduction

As concern about the adverse consequences of anthropogenic climate change has grown, so too has research into methods to reduce the emissions of greenhouse gases. Carbon dioxide storage could enable the continued use of fossil fuels with reduced CO_2 emissions. Storage in deep aquifers is among the most promising CO_2 storage options. The characteristics of a preferred storage site include: (i) high capacity to allow storage of large volumes of CO_2, (ii) high injectivity to allow injection at desired rates, and (iii) containment to ensure limited leakage (if any). Injectivity is not only a function of static reservoir properties (e.g., permeability and pay thickness), but also can change with time. This paper studies salt precipitation in the vicinity of the injection well, as one of the time-dependent phenomena that could affect injectivity. In particular, an analytical model is developed to estimate the radius of the dry-out zone – where salt precipitation occurs – and the fraction of the pore volume that will be occupied by salt. Our model is based on an extension of that developed by Orr (2007) for linear two-component, two-phase displacement. We apply this model to the problem of radial displacement of brine by CO_2. Although flow is not purely one-dimensional in actual field-scale, in the vicinity of the wellbore – where salt precipitation occurs – viscous forces dominate gravitational forces and flow may reasonably be approximated as one-dimensional.

In the following paragraphs, the physical problem is described. This is followed by development of a mathematical model for radial CO_2/brine binary displacement. Then, salt precipitation is formulated for the region where vaporization occurs in the binary system and is included in the model. Next, the effect of salt precipitation on permeability is studied and presented in terms of a time-dependent skin factor. Lastly, the analytical model is applied to a specific problem with an available numerical solution, enabling us to evaluate the effect of assumptions and approximations made in the development of the analytical solution.

* *Corresponding author.*
E-mail address: mzeidoun@ucalgary.ca (M. Zeidouni).

1750-5836/$ – see front matter © 2009 Elsevier Ltd. All rights reserved.
doi:10.1016/j.ijggc.2009.04.004

Nomenclature

A	cross-sectional area (m^2)
f	fractional flow
G	normalized global concentration (–)
h	aquifer thickness (m)
H	normalized molar rate (–)
k	permeability (Darcy)
m	number of moles (kmol)
q	volumetric rate (m^3/s)
r	radius (m)
R	spherical radius of close packed structure (m)
s	salinity (mole fraction)
$skin$	skin factor
S	saturation
t	time (s)
x	distance (m)
z	global mole fraction (fraction)

Greek letters

α	definition given by Eqs. (A.22a) and (A.22b)
η	similarity variable (m^2/s)
μ	viscosity (Pa s)
ρ	molar density ($kmol/m^3$)
ϕ	porosity (fraction)
ω	mole fraction

Subscripts

a	aqueous phase
dry	dry-out region
D	dimensionless
g	gaseous phase
inj	injection
r	relative
t	total
w	well
0	initial

Superscripts

a	downstream of the leading shock
b	upstream of the leading shock
c	downstream of the trailing shock
d	upstream of the trailing shock

2. Physical problem

Consider 1D CO_2 injection in an infinitely large saline aquifer through a well in the centre of the aquifer. The following is a possible phase arrangement: deep in the reservoir, where brine has not been in contact with injected CO_2, only fresh brine exists (region 1 in Fig. 1). In the region upstream of the fresh brine, the brine contains the CO_2 component. In this region, both aqueous and gaseous phases are mobile and in equilibrium (region 2 in Fig. 1). The gaseous phase saturation of this region is increasing toward the injection well. Moving further upstream toward the injection well, where the salinity level reaches that of halite-saturated brine, solid salt precipitation begins. Thus a region of three-phases (gaseous, aqueous, and solid) and three-components (water, CO_2, and salt) develops (region 3 in Fig. 1). In this region, the concentration of components in each phase is independent of total concentrations. The gaseous phase saturation increases toward the injection well while the aqueous phase saturation decreases. At a certain point, the aqueous phase flows slowly enough that it can be fully vaporized by the injected CO_2. This allows a two-phases (solid and gaseous) and three-components (water, CO_2, and salt) region to develop (region 4 in Fig. 1). Further upstream toward the injection well, the fresh injected CO_2 can transport the vaporized water outward. This allows development of a two-phases (solid and gaseous) and two-components (CO_2 and salt) dry-out region (region 5 in Fig. 1) (Fuller et al., 2006; Prévost et al., 2004).

3. Analytical model

Analytical modelling of the physical problem described above could consider a ternary system with three-phases (aqueous, gaseous, and solid) and three-components (CO_2, water, and salt). The problem of three-phase compositional flow has been studied in several publications (LaForce and Johns, 2005; LaForce et al., 2006). However, fully three-phase solutions are not simple to construct. Fortunately, since the system studied in this work is a limiting case of the more general ternary problem where one of the phases is immobile (the solid salt), a simplified solution is achievable. The physical problem is therefore approximated by a binary system with two-phases (aqueous and gaseous) and two-components (CO_2 and brine). In departure with the previous papers on the subject (Noh et al., 2007; Burton et al., 2008), we account for volume change upon mixing. Then, the amount of salt precipitation (solid phase saturation) is calculated separately based on the amount of vaporization. We then check the validity of this approximation by comparing the analytical results to the numerical ones for a specific case. The model assumes homogeneity, no diffusion/dispersion, no capillary and/or gravity forces, non-reactive rock, local phase equilibrium, and constant pressure and temperature.

In the following, the analytical model for the binary system is presented. The solution includes two shocks (discontinuities in saturation or concentration) that divide the medium into three regions. Far from the injection well – ahead of a leading shock – a fresh brine region exists that is being displaced by the injected CO_2. Upstream of the leading shock, a region of two-phase flow exists (an equilibrium region), in which an aqueous phase (brine and dissolved CO_2) and a gaseous phase (CO_2 and vaporized water) flow. A trailing evaporation shock separates the equilibrium region from the dry-out region closest to the wellbore where salt has precipitated. In this solution, the region arrangement reduces to that shown in Fig. 2. The assumptions that lead to these three regions are discussed later in this paper.

After analytical modelling of the binary system, the amount of salt that precipitates behind the trailing shock is included in the model. In the case of CO_2 storage in aquifers, salts can also precipitate through chemical reactions; however, the rock is assumed to be non-reactive in this study.

3.1. Analytical model for the binary system

The solution presented in this section considers a binary system composed of two-phases (aqueous and gaseous) and two-components (CO_2 and brine). The components transfer between the displacing injected gas and displaced aquifer brine. Therefore, the resulting aqueous phase includes brine with some dissolved CO_2. Similarly, the gaseous phase will contain *CO_2* and vaporized *brine*. In reality, although the gaseous phase will contain CO_2 and vaporized *water*, brine is used here instead, so that the flow problem is simplified to include only two-components. The assumption here is that salt and water act together. With this

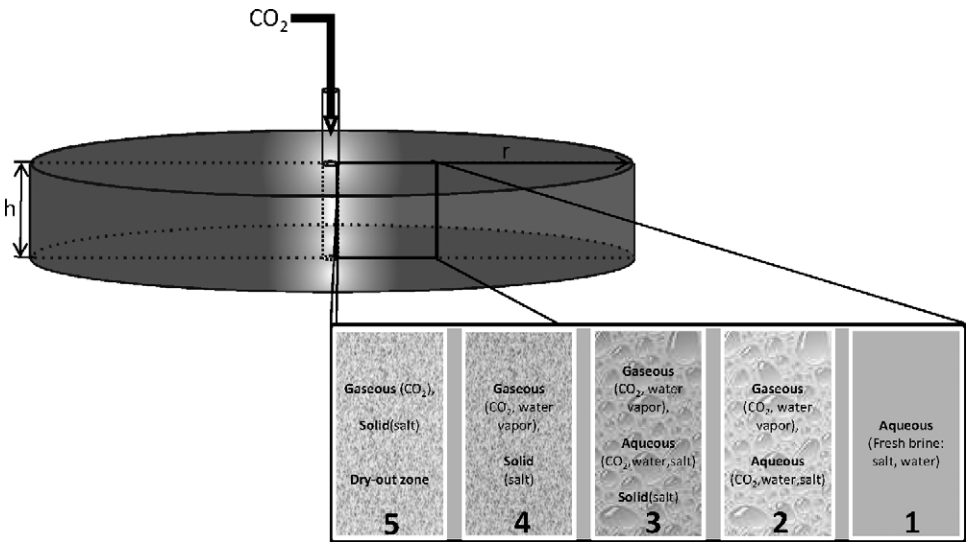

Fig. 1. Schematic of radial CO_2/brine displacement and arrangement of different phases.

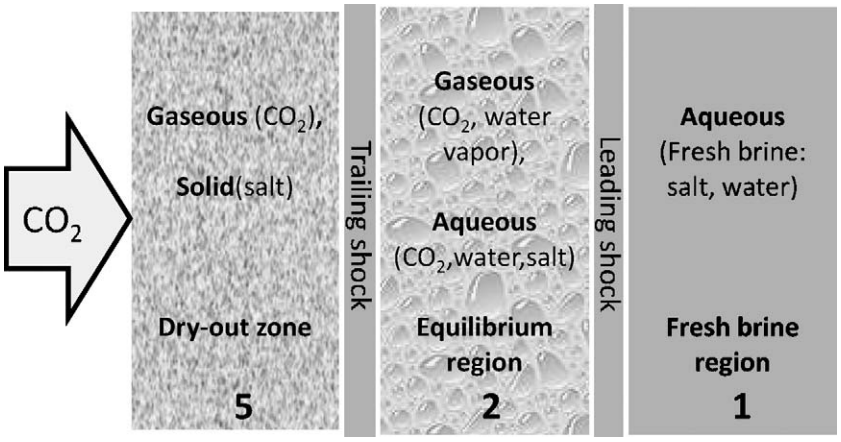

Fig. 2. Nomenclature and arrangement of phases for the analytical model presented in the paper.

assumption, the problem becomes similar to the gas/liquid displacement problem solved by many including Orr (2007). To correct for this assumption, the properties of water are assigned to brine in the gaseous phase. As mentioned earlier, once the flow problem with two-phases and two-components is solved, salt precipitation is added to the solution.

Appendix A gives the details of the solution. Starting with the continuity equation and using the fractional flow concept, one can obtain the following first-order nonlinear hyperbolic partial differential equation:

$$\frac{\partial G_{CO_2}}{\partial t} + \frac{q_{inj}}{\pi h \phi} \frac{dH_{CO_2}}{dG_{CO_2}} \frac{\partial G_{CO_2}}{\partial r^2} = 0 \quad (1)$$

where r and t are the radial coordinate and time, respectively. G_{CO_2} is total molar density (global concentration) of the CO_2 component normalized with respect to the molar density of injected fluid. H is total molar rate of CO_2 component normalized with respect to molar injection rate. A similar equation can also be written for the brine component. Eq. (1) is analogous to the Buckley–Leverett equation describing 1D displacement of one immiscible-phase by another (Eq. (2)) with a number of differences (Buckley and Leverett, 1942):

$$\frac{\partial S_g}{\partial t} + \frac{q_{inj}}{\phi A} \frac{df_g}{dS_g} \frac{\partial S_g}{\partial x} = 0 \quad (2)$$

The differences between Eqs. (1) and (2) include: (i) Eq. (1) is developed for a radial geometry, while Eq. (2) is for a linear one; (ii) Eq. (1) accounts for mass transfer and volume change upon mixing, while Eq. (2) ignores both effects. The latter difference leads to replacement of saturation (S_g) with normalized global concentration (G_{CO_2}) and fractional flow function (f_g) with normalized total molar rate (H_{CO_2}). With the assumptions of no gravity nor capillary forces, the gaseous phase fractional flow is obtained by:

$$f_g = \frac{1}{1 + (k_{ra}/k_{rg})(\mu_g/\mu_a)} \quad (3)$$

where k_{ra} and k_{rg} are the relative permeability of aqueous and gaseous phases, respectively, and depend only on gaseous phase saturation. μ_a and μ_g are the viscosity of aqueous and gaseous phases, respectively. Aqueous phase fractional flow will be $1 - f_g$.

The solution to Eq. (2) is given by (Buckley and Leverett, 1942):

$$\left(\frac{x}{t}\right)_{S_g} = \frac{q_{inj}}{\phi A}\left(\frac{d f_g}{dS_g}\right)_{S_g} \quad (4)$$

As shown in Appendix A, the solution to Eq. (1) is analogous to Eq. (4) and may be given by:

$$\left(\frac{r^2 - r_w^2}{t}\right)_{G_{CO_2}} = \frac{q_{inj}}{\pi h \phi}\left(\frac{dH_{CO_2}}{dG_{CO_2}}\right)_{G_{CO_2}} \quad (5a)$$

or

$$\left(\frac{r^2 - r_w^2}{t}\right)_{G_{CO_2}} = \frac{q_{inj}}{\pi h \phi}\left(q_D \frac{d f_g}{dS_g}\right)_{G_{CO_2}} \quad (5b)$$

where r_w is the wellbore radius, $q_D = q_t/q_{inj}$, and q_t is the total local flow rate, defined as the summation of aqueous and gaseous phase flow rates. In the solution given by Eq. (5), where mass transfer occurs between phases and there is volume change upon mixing, q_t is not equal to q_{inj}, and varies between different regions. Eq. (5) gives the wave velocity $\eta = (r^2 - r_w^2)/t$ of any specific G_{CO_2}. Therefore, each gaseous phase saturation, S_g, travels at a constant velocity given by Eq. (5), since there is a one-to-one relationship between G_{CO_2} and S_g (as shown in Appendix A by Eq. (A.8.2). Note that the problem has a similarity property and the solution is expressed in terms of gaseous phase saturation or CO_2 overall mole fraction versus the similarity variable (wave velocity). The solution given by direct use of Eq. (5) is physically impossible because of multiple saturation values at a single location. Ignoring the capillary pressure (and also the diffusion process) give rise to this multi-valued solution. We recall that this problem also occurs when solving the conventional Buckley–Leverett equation (Eq. (2)). The inconsistency has been resolved by introducing a shock that connects the two different regions of the solution. In the problem presented in this paper, three regions are formed. As such, two shocks will be required to connect the regions: the trailing shock and the leading shock. The trailing shock is the shock which connects the two-phase gaseous/solid region to the two-phase gaseous/aqueous region. The shock that connects the two-phase gaseous/aqueous region to the single-phase aqueous region is called the leading shock, as it is always ahead of the trailing shock.

In locating the shocks, we use the following as boundary and initial conditions:

$$\begin{cases} S_g = 0 \quad \text{at } t = 0, \ r > 0 & \text{(a)} \\ S_g = 1 \quad \text{at } t > 0, \ r = r_w & \text{(b)} \end{cases} \quad (6)$$

3.2. Solution and its graphical representation

The solution of the problem is obtained by solving for: the saturation downstream of the trailing shock (S_g^c), the saturation upstream of the leading shock (S_g^b), and the dimensionless local flow rate between the shocks (q_D). The wave velocity of these saturations and all saturations in between is obtained by Eq. (5). As shown in Appendix A, Eqs. (7) and (8) can be solved simultaneously to obtain S_g^c (the gas saturation downstream of the trailing shock), and q_D^c (the dimensionless local flow rate downstream of the trailing shock):

$$q_D^c = \frac{\alpha^d_{Brine}(G^d_{CO_2} - G^c_{CO_2}) - \alpha^d_{CO_2}(G^d_{Brine} - G^c_{Brine})}{\alpha^c_{Brine}(G^d_{CO_2} - G^c_{CO_2}) - \alpha^c_{CO_2}(G^d_{Brine} - G^c_{Brine})} \quad (7)$$

$$q_D^c \frac{d f_g}{dS_g} = \frac{\alpha^d_{CO_2} - q_D^c \alpha^c_{CO_2}}{G^d_{CO_2} - G^c_{CO_2}} \quad (8)$$

In the equations above, $G^d_{CO_2}$ and G^d_{Brine} are known and $G^c_{CO_2}$ and G^c_{Brine} are functions of S_g^c only. Having obtained q_D^c and S_g^c, we can find the location of the shock based on Eq. (5).

The leading shock is located by simultaneous solution of Eqs. (9) and (10) to obtain S_g^b (the gas saturation upstream of the leading shock):

$$\frac{q_D^a}{q_D^b} = \frac{\alpha^b_{CO_2}(G^a_{Brine} - G^b_{Brine}) - \alpha^b_{Brine}(G^a_{CO_2} - G^b_{CO_2})}{\alpha^a_{CO_2}(G^a_{Brine} - G^b_{Brine}) - \alpha^a_{Brine}(G^a_{CO_2} - G^b_{CO_2})} \quad (9)$$

$$q_D^b \frac{d f_g}{dS_g} = \frac{q_D^a \alpha^a_{CO_2} - q_D^b \alpha^b_{CO_2}}{G^a_{CO_2} - G^b_{CO_2}} \quad (10)$$

Note that $q_D^b = q_D^c$, since the flow velocity is constant in the two-phase region (Dumore et al., 1984). q_D^c is already obtained from the solution for the trailing shock. Having obtained S_g^b, we can find the location of the leading shock based on Eq. (5).

For the case of pure CO_2 injection in an aquifer that initially contains only brine (i.e., no dissolved CO_2), the placement of the shocks could be determined graphically. The method uses the gaseous phase fractional flow versus the gaseous phase saturation curve (f_g–S_g curve) to obtain the saturation at the trailing and leading shocks. The method is illustrated in Fig. 3. Gaseous phase saturation downstream of the trailing shock can be found by drawing a line from point J tangent on the f_g–S_g curve. A tangent line drawn from point I on the f_g–S_g curve gives the gaseous phase saturation upstream of the leading shock. Both points I and J are located on a unit slope line drawn from the origin and can be obtained by:

$$(S_g^I, f_g^I) = \left(\frac{\rho_{aD}\omega_{CO_2,a}}{\rho_{aD}\omega_{CO_2,a} - \rho_{gD}\omega_{CO_2,g}}, \frac{\rho_{aD}\omega_{CO_2,a}}{\rho_{aD}\omega_{CO_2,a} - \rho_{gD}\omega_{CO_2,g}}\right) \quad (11)$$

$$(S_g^J, f_g^J) = \left(\frac{\rho_{aD}\omega_{Brine,a}}{\rho_{aD}\omega_{Brine,a} - \rho_{gD}\omega_{water,g}}, \frac{\rho_{aD}\omega_{Brine,a}}{\rho_{aD}\omega_{Brine,a} - \rho_{gD}\omega_{water,g}}\right) \quad (12)$$

To determine the similarity variable at the shock (based on Eq. (5)), the local flow rate at the two-phase region (q_D^c) is required; it is obtained by:

$$q_D^c = \frac{(\rho_{aD}\omega_{CO_2,a} - \rho_{gD}\omega_{CO_2,g})S_g^c - \Delta\rho_D S_g^c + \omega_{Brine,a}\rho_{aD}}{(\rho_{aD}\omega_{CO_2,a} - \rho_{gD}\omega_{CO_2,g}) f_g^c - \Delta\rho_D f_g^c + \omega_{Brine,a}\rho_{aD} + \rho_{aD}\rho_{gD}\Delta\omega_{CO_2}(S_g^c - f_g^c)} \quad (13)$$

where: $\Delta\rho_D = \rho_{aD} - \rho_{gD}$ and $\Delta\omega_{CO_2} = \omega_{CO_2,a} - \omega_{CO_2,g}$.

For all the saturations between the trailing shock and leading shock, the similarity variable could be obtained based on Eq. (5). The details of the derivation of the above graphical method are given in Appendix A. The application of this solution to problems of CO_2 injection into aquifers is given later on in this paper.

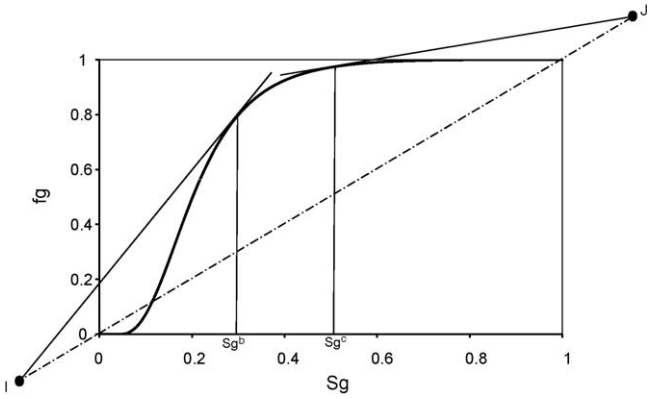

Fig. 3. Graphical method to determine the specifications (saturations and similarity variables) of the trailing and leading shocks.

In summary, the solution consists of three regions: a single-phase gaseous region, a two-phase region of gaseous and aqueous phases, and a region of brine at its initial condition. Capillary pressure and gravity forces are ignored in this analytical work due to the complexity added to the solution. In the presence of capillary pressure and gravity forces and with a strong viscous force (such as close to wellbore), development of a shock-like solution has been shown in the literature (Bruining, 2001; Fayers and Sheldon, 1959).

3.3. Salt precipitation in the dry-out zone

In this section, salt precipitation is modelled and included in the radial CO_2/brine displacement described above. Salt precipitation may occur due to vaporization of brine into the gaseous phase during CO_2 injection. When CO_2 comes in contact with brine, some CO_2 dissolves in the brine, and some water vaporizes into the flowing gas phase, which then displaces brine. The amount of brine that is displaced in the zone of two-phase flow is less than the total movable brine saturation. Since the brine is being vaporized while it is moving, the displaced brine saturation will be less than the movable brine saturation. The higher the mobility of the brine, the more brine is displaced and the less chance for vaporization. We approximate the three-component (CO_2, water, and salt) system with a two-component (CO_2 and brine) system to construct the saturation profile. The analytical solution is found to be composed of three regions that are connected by two shocks (trailing and leading). The trailing shock velocity was found to be the same as the velocity of the brine saturation downstream. Therefore, all the saturations with velocities lower than the trailing shock velocity will not appear in the solution. The brine will be fully vaporized once it reaches the saturation downstream of the trailing shock. The gaseous phase which enters the equilibrium region is saturated by water.

Displacement of the fresh brine by the gaseous phase allows propagation of the leading shock. The brine behind the leading shock is already saturated by CO_2. As such, there is no mass transfer between the saturated aqueous phase behind the leading shock and saturated gaseous phase ahead of the trailing shock. In other words, in this model there is no salinity change in the equilibrium region. Hence, all the solid salt precipitation will occur upstream of the trailing shock as a result of vaporizing the saturated brine downstream of the trailing shock (i.e., where $S_a^c = 1 - S_g^c$). This region is known as the dry-out zone. Static material balance calculations give the equation below for the solid salt saturation in the dry-out region (See Appendix C for details):

$$S_{salt} = \frac{\rho_a \omega_{salt,a}}{\rho_{salt}}(1 - S_g^c) \tag{14}$$

Eq. (14) suggests that the precipitated salt saturation depends on molar salt concentration in the aqueous phase ($\omega_{salt,a}$), aqueous phase density (ρ_a), solid salt density (ρ_{salt}), and the gas saturation downstream of the trailing shock (S_g^c). In practice $\omega_{salt,a}$ may not be available. However, it can be closely approximated based on the brine salinity (See Appendix C for details):

$$\omega_{salt,a} = s(1 - \omega_{CO_2,a}) \tag{15}$$

3.4. Porosity and permeability change

Due to salt precipitation, the porosity decreases based on Eq. (16):

$$\phi = \phi_0(1 - S_{salt}) \tag{16}$$

Salt may precipitate in the large pores or in the small pores, in pore bodies or in pore throats. Depending on where the salt is precipitated, it may or may not significantly affect the permeability. Many models have been presented to relate permeability to porosity (Nelson, 1994). In this study, we use a simple Kozeny–Carman grain model based on spheres to calculate changes in permeability due to changes in porosity (Bolton et al., 1999). In essence, this equation will estimate the permeability of media based on a grain size distribution. This equation is given by:

$$k = \frac{R_0^2}{45}\left(\frac{\phi^3}{(1-\phi)^2}\right) \tag{17}$$

where R_0 is the initial local spherical radius in close packed structure.

Hence, the ratio of the permeability k to initial permeability k_0 can be expressed as:

$$\frac{k}{k_0} = \left(\frac{\phi}{\phi_0}\right)^3\left(\frac{1-\phi_0}{1-\phi}\right)^2 \tag{18}$$

where ϕ_0 is the initial porosity. Combining Eqs. (16) and (18) gives:

$$\frac{k}{k_0} = \frac{(1 - S_{salt})^3}{(1 + (\phi_0/(1-\phi_0))S_{salt})^2} \tag{19}$$

Since the solid salt saturation in the dry-out zone is constant, the permeability reduction in the dry-out zone is independent of radius. However, with the expansion of the dry-out zone with time, the permeability reduction affects an increasingly larger area of the aquifer.

3.5. Skin factor

The change in permeability can be described by a skin factor which may be included in injectivity calculations (Hawkins, 1956):

$$\text{skin} = \int_{r_w}^{r}\left(\frac{k_0}{k} - 1\right)\frac{dr}{r} \tag{20}$$

Combining Eqs. (19) and (20) gives:

$$\text{skin} = \left(\frac{(1 + (\phi_0/(1-\phi_0))S_{salt})^2}{(1 - S_{salt})^3} - 1\right)\ln\left(\frac{r_{dry}(t)}{r_w}\right) \tag{21}$$

where r_{dry} is the radius of the dry-out region which is time-dependent. Therefore, Eq. (21) gives skin as a function of time.

4. Model verification

The analytical solution of this paper assumes homogeneity, no diffusion/dispersion, no capillary nor gravity forces, non-reactive rock, local phase equilibrium, and constant pressure and temperature. Moreover, the analytical model approximates the ternary system with a binary system in which salt precipitation only occurs within the dry-out zone. The analytical model described above is now applied to a reference case from the literature which is solved numerically. The numerical results are based on a totally different formulation that does not have these constraining assumptions nor approximations. Therefore, comparison between analytical and numerical results can help to investigate the relevancy of our assumptions and approximations.

4.1. Reference case

The overall effect of salt precipitation on the permeability has been experimentally examined by Muller et al. (2008). However, the permeability change has not been spatially reported, so those results cannot be compared to the analytical solution. Moreover, the capillary effect may not have been minimised in the experimental data, again making it difficult to compare to the

Table 1
Aquifer data.

	Reference case	Higher salinity case
Brine salinity (mole fraction)	0.0516	0.0931
Aquifer temperature (°C)	45	35
Aquifer pressure (MPa)	12	7.5
Porosity, fraction	0.12	0.2
Injection rate (kg/s)	100	1
Aquifer thickness (m)	100	30
Viscosity of gaseous phase (cp)	0.0496	0.0412
Viscosity of aqueous phase (cp)	0.8260	1.3647
Connate water saturation (fraction)	0.3	0.1
Critical gaseous phase saturation (fraction)	0.05	0.0
Equilibrium mole fraction of CO_2 in gaseous phase, $\omega_{CO_2,g}$	0.9953	0.9980
Equilibrium mole fraction of CO_2 in aqueous phase, $\omega_{CO_2,a}$	0.0110	0.0065
CO_2 mole fraction in injected gaseous phase, $\omega_{CO_2,g}$	1	1
Initial CO_2 mole fraction in aquifer brine, $\omega_{CO_2,a}$	0	0
Initial brine density (kmol/m^3)	54.8527	54.3784
Injected CO_2 density (kmol/m^3)	14.6126	8.4926
Equilibrium aqueous phase density (kmol/m^3)	54.3046	54.0559
Equilibrium gaseous phase density (kmol/m^3)	14.6846	8.5119
Solid salt molecular weight (kg/kmol)	58.43	58.43
Solid salt molar density (kmol/m^3)	37.05	37.05
Well radius (m)	0	0.1

analytical solution, where one of the assumptions is no capillary force. The analytical model is instead applied to a problem with a numerical solution: CO_2 injection into a saline aquifer with simplified flow geometry and aquifer properties. CO_2 is injected into a homogeneous, isotropic, infinite-acting aquifer at conditions of 120 bar pressure, 45 °C temperature, and a salinity of 15 wt.%. CO_2 is injected at a constant rate of 100 kg/s in the aquifer centre through a well which is completed over the entire aquifer thickness of 100 m. The flow is assumed to be 1D radial and gravity effects are neglected. This problem has been presented in the Lawrence Berkeley National Laboratory inter-comparison project (Pruess et al., 2002) as test Problem #3. Detailed specifications for this problem are given in Table 1. The aqueous and gaseous phase relative permeability curves are obtained based on the models given in Table 2. The numerical results for this problem are presented by Pruess and Spycher (2007), using a TOUGH2 simulator with the ability to simulate the salt precipitation. The PVT data used in the numerical work is based on the PVT model presented by Spycher and Pruess (2005).

4.2. Analytical solution

In development of the analytical solution, the radial CO_2/brine model is used first to locate the trailing and leading shocks. We also use this model to find the profiles of gaseous phase saturation and CO_2 mole fraction. The gaseous phase fractional flow versus gaseous phase saturation (f_g–S_g) is plotted first (Fig. 4). Points *I* and *J* are obtained based on Eqs. (11) and (12). Tangent lines from these points on the fractional flow curve give 0.198 and 0.489 for the gaseous phase saturation upstream of the leading shock and downstream of the trailing shock, respectively. The profiles of gaseous phase saturation and global CO_2 mole fraction are illustrated in Figs. 5 and 6. Based on these figures, the radius of dry-out region will reach 60 m after 10 years of injection in this case. At that time, the CO_2 front will be at 2206 m from the injector.

Using the formulation presented in this paper, the solid salt saturation is calculated to be 0.038 in the dry-out zone. For thermodynamic calculations in the analytical solution, we have used the PVT model of Hassanzadeh et al. (2008), which is in close agreement with that of Spycher and Pruess (2005).

Table 2
Relative permeability curves.

Aqueous: van Genuchten function (1980) $k_{ra} = \sqrt{S^*}\left(1-\left(1-[S^*]^{1/\lambda}\right)^{\lambda}\right)^2$ where : $S^* = \frac{S_a - S_{wirr}}{1-S_{wirr}}$ and $\lambda = 0.457$

Gaseous: Corey curve (1954) $k_{rg} = (1-\hat{S})^2(1-\hat{S}^2)$ where : $\hat{S} = \frac{S_a - S_{wirr}}{1-S_{wirr}-S_{gc}}$

4.3. Comparison of the analytical model with the numerical results

Pruess and Spycher (2007) have shown that the numerical results for the reference case follow a similarity solution, where the solution remains invariant when plotted versus the similarity variable r^2/t (note that the numerical results are given for the line source case; i.e., for $r_w = 0$). This is in agreement with the findings of the analytical solution developed in this paper. The analytical versus numerical results are shown in Figs. 7 and 8 with respect to the similarity variable. The following differences are observed. The simulation results exhibit fluctuating solid salt saturation in the dry-out zone, which on average agree with the analytical solution. Furthermore, the numerical model gives a somewhat slower leading shock and a faster trailing shock. As the pressure varies in the numerical simulation, the compositional properties change as well. This therefore leads to subtle differences between the shock locations and saturations of the numerical and analytical solutions.

Salt precipitation occurs behind the trailing shock (dry-out zone) only. Based on Eq. (19), the permeability of the dry-out zone reduces to 0.87 of its initial value due to salt precipitation. Assuming a wellbore radius of 0.1 m, skin factor will be about 0.76 after the first year, increasing slowly to reach a value of about 1.0 after 25 years (Fig. 9).

If the analytical model is applied to the problem above with halite-saturated brine (salinity of 30 wt.%), the solid salt saturation can be as high as 0.086 in such a case. As a result, the permeability reduces to 0.73 of its initial value due to salt precipitation.

4.4. Higher salinity case

The following example is presented based on the information given by Hurter et al. (2008) for the CO2SINK project in Ketzin, Germany in the Stuttgart formation.

CO_2 is injected at a rate of 1 kg/s in an aquifer with 0.2 porosity, 200 mD permeability, and 30 m thickness. The aquifer is initially at 7.5 MPa pressure and 35 °C temperature. The formation brine is highly saline (250,000 ppm), which we assume to be saturated. Further information on this problem is given in Table 1.

Using Eq. (14), we obtain the solid salt saturation of 0.03 in the dry-out zone. The result of applying the analytical model to this case is shown in Fig. 10. The dry-out region radius after two years is 3.9 m based on the analytical solution, compared to 13 m given by Hurter et al. (2008).

We can use Eq. (19) to calculate the change in permeability. Fig. 11 shows the ratio of current to initial permeability versus aquifer radius for different times. A region of 12 m radius will be affected by salt precipitation after 20 years.

The permeability in the dry-out zone reduces to 0.89 of the initial permeability. The change in permeability due to salt precipitation can be illustrated by a time-dependent skin factor based on Eq. (21). Fig. 12 shows the skin factor of the injection well versus time for the first 25 years of injection. The skin factor increases quickly over early years of injection and reaches 0.6.

5. Discussion

The analytical model presented here is based on the approximation of the ternary system by a binary model. We also neglect

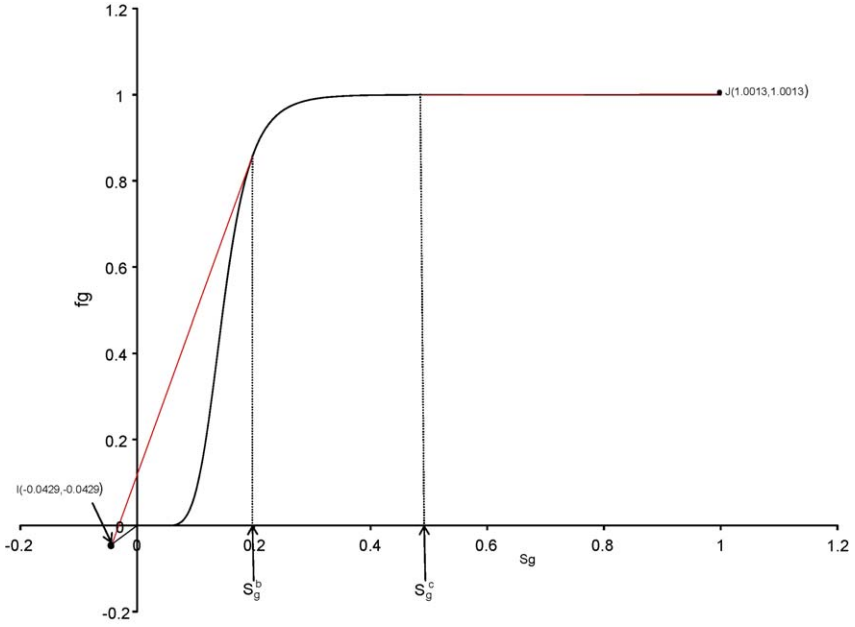

Fig. 4. Determination of specifications of the shocks for the base case.

capillary and gravity forces in developing the model. Inclusion of capillary pressure would cause counter-current imbibition of brine into blocks with low brine saturation. This can be of significant importance if injection rate is small, or when due to a combination of gravity forces and/or heterogeneity, regions of low velocity occur where capillary forces could play a significant role. This capillary effect would move more brine into the region where dry-out occurs. Thus, neglecting the capillary force in some situations may significantly underestimate the local amount of salt precipitation. The results presented in this paper indicated that reduction in permeability due to salt precipitation can be relatively small when capillary and gravity forces are neglected. However, if solid salt perfectly plugs the pore throats, permeability reduction may be more severe (Kleinitz et al., 2001).

Since completion of this work, Pruess and Muller (2009) and Pruess (2009) have presented numerical and analytical studies of salt precipitation. The numerical studies of Pruess and Muller (2009) use gas–water relative permeability curves with a large curvature leading to precipitation of up to 9.1% salt. When this is combined with a permeability model that exhibits complete plugging (zero permeability) at 10%, significant pressure drop close to the wellbore is observed. In their 2D simulation studies, Pruess and Muller (2009) show that in the presence of gravity, CO_2 override could lead to regions of low velocity at the bottom of formation. In such a region, where the viscous force is small, the capillary force causes significant brine supply to the dry-out zone with salt saturation as high as 20% observed in the numerical results.

1D numerical results are not available to be compared with the results of the analytical model for the higher salinity case (Stuttgart formation). However, 2D numerical results for this problem are given by Hurter et al. (2008). Values as high as 0.8 are reported for the solid salt saturation using the numerical simulation, compared to a maximum of 0.03 for the solid salt saturation predicted by the 1D analytical model. This is a significant difference between the 2D numerical and 1D analytical results. One of the reasons for this difference could be related to the combined effect of capillary and gravity forces as described above. In situations where salt precipitation may be a concern, a preflush treatment could displace the high salinity brine away from the wellbore, alleviating the problems associated with potential plugging in the near wellbore region (Pruess and Muller, 2009).

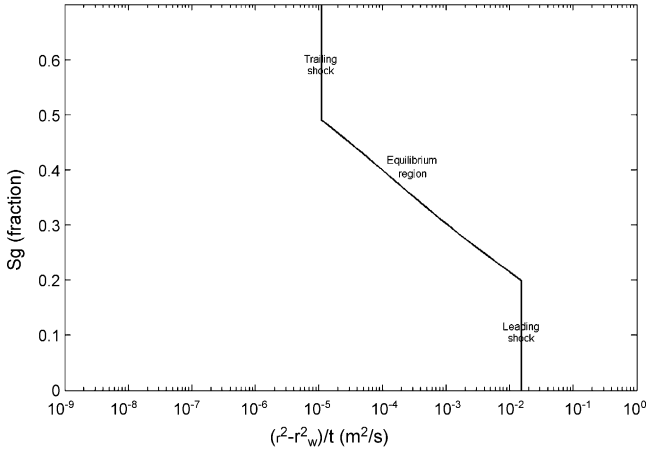

Fig. 5. Analytical gaseous phase saturation profile (salt precipitation neglected).

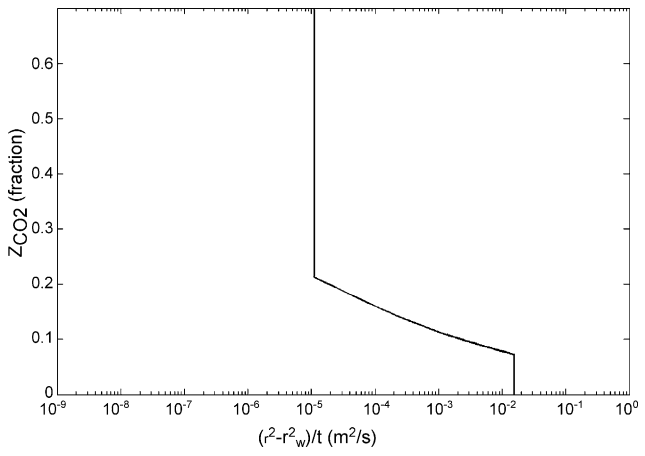

Fig. 6. Analytical global CO_2 mole fraction profile (salt precipitation neglected).

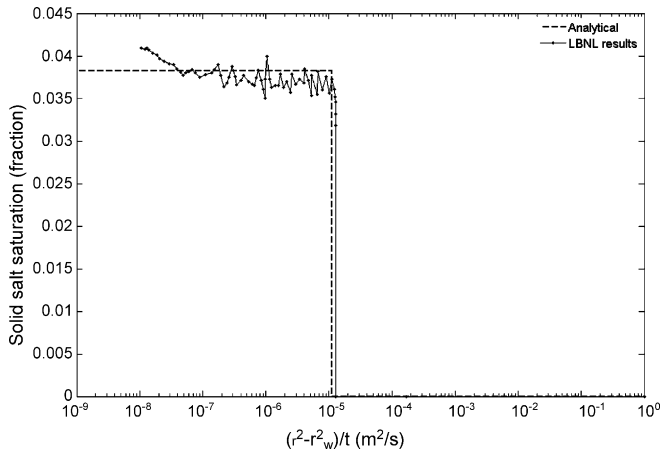

Fig. 7. Analytical versus numerical results for solid salt saturation.

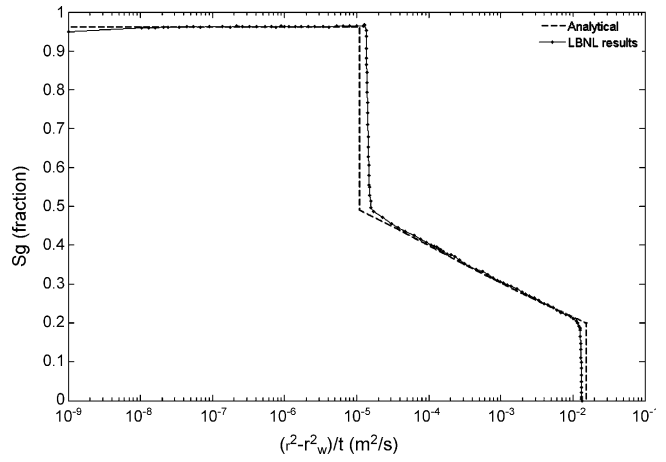

Fig. 8. Analytical versus numerical results for gaseous phase saturation.

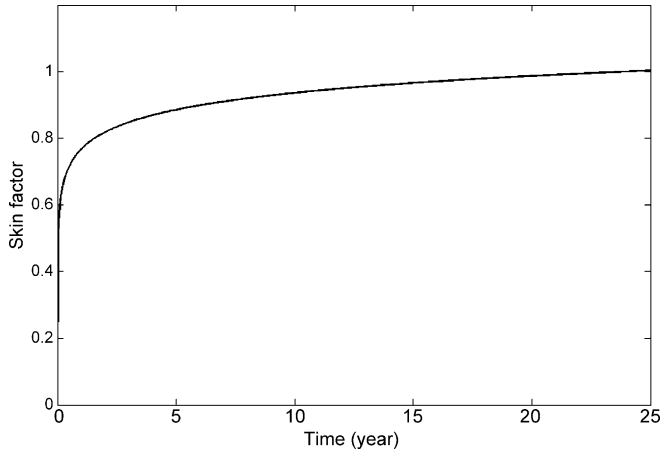

Fig. 9. The skin factor of injection well over time for reference case assuming $r_w = 0.1$ m.

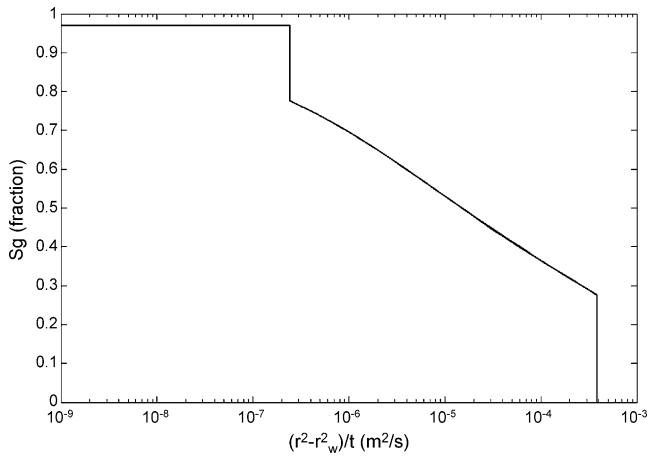

Fig. 10. Analytical results for gaseous phase saturation of higher salinity case.

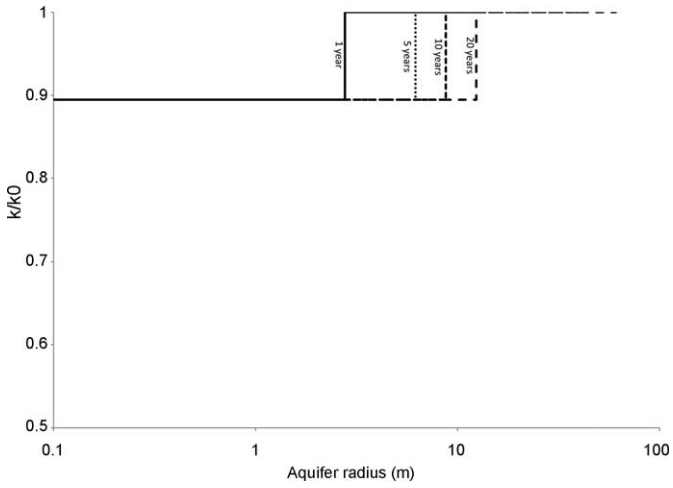

Fig. 11. Analytical results for permeability reduction of higher salinity case.

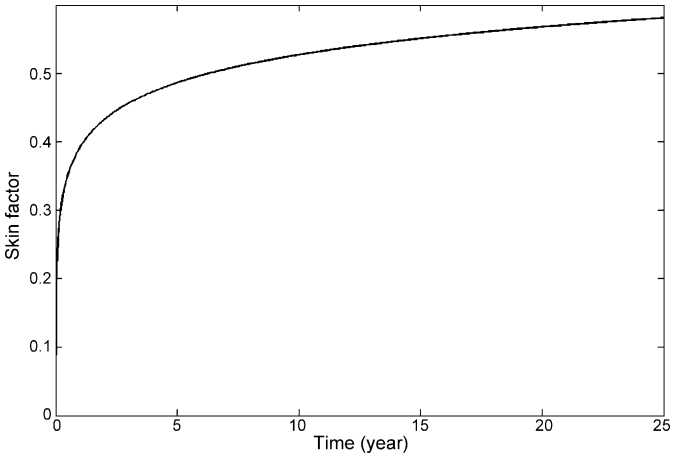

Fig. 12. The skin factor of injection well over time for higher salinity case.

Wellbore injectivity is certainly not controlled by salt precipitation alone. During CO_2 injection in an aquifer, the more viscous phase (formation water) is displaced by a less viscous phase (CO_2), so the reduction in injectivity due to salt precipitation can be offset (at least partially) by increased mobility as a result of the replacement of water by CO_2 in the near wellbore region.

6. Summary and conclusions

Due to salt precipitation, as water evaporates into injected CO_2, porosity and permeability might be reduced in some CO_2 injection scenarios. An analytical model is developed to predict the amount of salt precipitation and the region in which it occurs over time. The

model assumes homogeneity, no diffusion/dispersion, no gravity nor capillary forces, non-reactive rock, local phase equilibrium, and constant pressure and temperature. In developing this model, Orr's formulation for two-component CO_2/brine displacement is applied to a radial coordinate system. Next, a model for salt precipitation is developed and included in the radial two-phase model. In derivation of the model, it is shown that it has a similarity property; the solution depends on radial distance r and time t only through the similarity variable $\eta = (r^2 - r_w^2)/t$. The similarity variable η, known as wave velocity, is the local flow rate times the fractional flow derivative. This definition of wave velocity gives a physically impossible solution because we find that more than one saturation will exist at a single location. The inconsistency is resolved by the propagation of discontinuities known as shocks. Approximation of the ternary system by a binary system gives rise to the prediction that salt precipitation occurs in the region behind the trailing shock (dry-out zone) only. Salt precipitation in the dry-out zone occurs because of vaporization of the brine saturation corresponding to downstream of the trailing shock. The model is extended to evaluate the effect of salt precipitation on porosity and permeability. It is also shown that the effect can be described in terms of time-dependent skin factor.

The analytical model was applied to the Lawrence Berkeley National Laboratory inter-comparison Problem #3 (Pruess et al., 2002). The analytical results match the numerical results provided by Pruess and Spycher (2007) using the TOUGH2 simulator as indicated in Figs. 7 and 8. In such a case, the permeability may reduce to 87% of its initial value.

For cases studied, salt saturation was a few percent. The loss in injectivity depends on the degree of reduction of formation permeability with increased salt saturation. For permeability-reduction models considered in this work, the loss in injectivity was not severe.

Acknowledgements

The authors would like to thank Hassan Hassanzadeh for providing his PVT model and helpful discussions. The authors also wish to thank Yuri Leonenko for input on the numerical solution. The authors also wish to express their grateful appreciation for useful comments of the reviewers that led to significant improvement of the paper.

Appendix A. Radial two-component CO_2/brine displacement

In the following, a model for radial CO_2/brine displacement is developed. CO_2 is injected in a well of radius r_w, which is placed in the centre of an infinite-acting brine aquifer. Starting with the continuity equation and using the concept of fractional flow, Orr (2007) developed a linear two-component gas/oil displacement model; the model developed here is the radial two-component CO_2/brine displacement analog of Orr (2007).

The continuity equations in 1D radial flow for each of aqueous (=a) and gaseous (=g) phases are:

$$-\frac{\partial(\rho_a q_a)}{\partial r} = \frac{\partial}{\partial t}(A\phi\rho_a S_a) \tag{A.1}$$

$$-\frac{\partial(\rho_g q_g)}{\partial r} = \frac{\partial}{\partial t}(A\phi\rho_g S_g) \tag{A.2}$$

Summation of Eqs. (A.1) and (A.2) gives:

$$-\frac{\partial}{\partial r}(\rho_a q_a + \rho_g q_g) = \frac{\partial}{\partial t}(A\phi\rho_a S_a + A\phi\rho_g S_g) \tag{A.3}$$

For the CO_2 component in each of the phases, we may write the following considering no diffusion:

$$-\frac{\partial}{\partial r}(\rho_a \omega_{CO_2,a} q_a + \rho_g \omega_{CO_2,g} q_g) = \frac{\partial}{\partial t}(A\phi\rho_a \omega_{CO_2,a} S_a + A\phi\rho_g \omega_{CO_2,g} S_g) \tag{A.4}$$

Using the concept of fractional flow, where $f_a = q_a/q_t$ and $f_g = q_g/q_t$, we can write Eq. (A.4) as:

$$-\frac{\partial}{\partial r}(\rho_a \omega_{CO_2,a} f_a q_t + \rho_g \omega_{CO_2,g} f_g q_t) = \frac{\partial}{\partial t}(A\phi\rho_a \omega_{CO_2,a} S_a + A\phi\rho_g \omega_{CO_2,g} S_g) \tag{A.5}$$

Considering constant injection rate and porosity gives:

$$-\frac{q_{inj}}{A\phi}\frac{\partial}{\partial r}(\rho_{aD} \omega_{CO_2,a} f_a q_D + \rho_{gD} \omega_{CO_2,g} f_g q_D) = \frac{\partial}{\partial t}(\rho_{aD} \omega_{CO_2,a} S_a + \rho_{gD} \omega_{CO_2,g} S_g) \tag{A.6}$$

where $q_D = q_t/q_{inj}$ and $\rho_{aD} = \rho_a/\rho_{inj}$ and $\rho_{gD} = \rho_g/\rho_{inj}$.

In this equation, the flow rates and the densities of liquid and gas phases are made dimensionless, based on injected fluid values. q_t is the local flow rate, which is the summation of local liquid and gas flow rates. Due to the volume change as components transfer between phases, the local flow rate of each of the phases varies. Therefore, the local flow rate is not constant. $\omega_{CO_2,a}$ and $\omega_{CO_2,g}$ are the equilibrium mole fractions of CO_2 component in the liquid and gas phases, respectively. The mole fractions and densities are fixed, because the pressure and temperature are taken as constant. Eq. (A.6) can be re-written as:

$$-\frac{q_{inj}}{A\phi}\frac{\partial H_{CO_2}}{\partial r} = \frac{\partial G_{CO_2}}{\partial t} \tag{A.7}$$

where:

$$H_{CO_2} = \rho_{aD} \omega_{CO_2,a} f_a q_D + \rho_{gD} \omega_{CO_2,g} f_g q_D \tag{A.8.1}$$

$$G_{CO_2} = \rho_{aD} \omega_{CO_2,a} S_a + \rho_{gD} \omega_{CO_2,g} S_g \tag{A.8.2}$$

Replacement of the cross-sectional area $A = 2\pi rh$ gives:

$$-\frac{q_{inj}}{\pi h\phi}\frac{1}{2r}\frac{\partial H_{CO_2}}{\partial r} = \frac{\partial G_{CO_2}}{\partial t} \tag{A.9}$$

or:

$$\frac{\partial G_{CO_2}}{\partial t} + \frac{q_{inj}}{\pi h\phi}\frac{\partial H_{CO_2}}{\partial r^2} = 0 \tag{A.10}$$

A similar equation can also be written for the brine component. The above-noted assumption of constant pressure and temperature leading to phase densities and component mole fractions being fixed also leads to G_{CO_2} being a function of saturation only. Dumore et al. (1984) demonstrated that the local flow velocity is constant for composition variations along a single tie-line in the two-phase region. Therefore, H_{CO_2} is a function of gaseous phase fractional flow (f_g) only. In turn, f_g is a function of gaseous phase saturation (S_g) only. Thus, H_{CO_2} can be written in terms of G_{CO_2} only. The chain rule can be used to re-write Eq. (A.10) as:

$$\frac{\partial G_{CO_2}}{\partial t} + \frac{q_{inj}}{\pi h\phi}\frac{dH_{CO_2}}{dG_{CO_2}}\frac{\partial G_{CO_2}}{\partial r^2} = 0 \tag{A.11}$$

From Eq. (A.11), we conclude:

$$\left(\frac{dr^2}{dt}\right)_{G_{CO_2}} = \frac{q_{inj}}{\pi h\phi}\left(\frac{dH_{CO_2}}{dG_{CO_2}}\right)_{G_{CO_2}} \tag{A.12}$$

Integration of this equation gives:

$$\frac{r^2 - r_w^2}{t} = \frac{q_{inj}}{\pi h\phi}\frac{dH_{CO_2}}{dG_{CO_2}} \tag{A.13}$$

Next, we evaluate the term dH_{CO_2}/dG_{CO_2} to sketch the solution. Differentiation of Eqs. (A.8.1) and (A.8.2) gives:

$$\frac{dH_{CO_2}}{dG_{CO_2}} = q_D(\rho_{gD}\omega_{CO_2,g} - \rho_{aD}\omega_{CO_2,a})\frac{df_g}{dG_{CO_2}} \tag{A.14}$$

On the other hand:

$$\frac{df_g}{dG_{CO_2}} = \frac{df_g}{dS_g}\frac{dS_g}{dG_{CO_2}} = \frac{1}{\rho_{gD}\omega_{CO_2,g} - \rho_{aD}\omega_{CO_2,a}}\frac{df_g}{dS_g} \tag{A.15}$$

Substitution of Eq. (A.15) into Eq. (A.14) gives:

$$\frac{dH_{CO_2}}{dG_{CO_2}} = q_D\frac{df_g}{dS_g} \tag{A.16}$$

Then we have:

$$\left(\frac{r^2 - r_w^2}{t}\right)_{G_{CO_2}} = \frac{q_{inj}}{\pi h\phi}\left(q_D\frac{df_g}{dS_g}\right)_{G_{CO_2}} \tag{A.17}$$

The variable $\eta = (r^2 - r_w^2)/t$ is the wave velocity or similarity variable. In the definition of fractional flow, the gravity and capillary forces are neglected, so the following is obtained for gaseous phase fractional flow (Buckley and Leverett, 1942):

$$f_g = \frac{1}{1 + (k_{ra}/k_{rg})(\mu_g/\mu_a)} \tag{A.18}$$

where k_{rl} and k_{rg} are the relative permeabilities of aqueous and gaseous phases, respectively, that depend only on phase saturation. μ_l and μ_g are the viscosities of aqueous and gaseous phases, respectively. Since G_{CO_2} and fractional flow derivative are both functions only of gaseous phase saturation, the solution will be obtained in terms of gaseous phase saturation versus similarity variable, $\eta = (r^2 - r_w^2)/t$. This solution can be converted to an expression of overall mole fraction, using the equation below, also versus the similarity variable:

$$z_{CO_2} = \frac{\rho_{gD}\omega_{CO_2,g}S_g + \rho_{aD}\omega_{CO_2,a}S_a}{\rho_{gD}S_g + \rho_{aD}S_a} \tag{A.19}$$

However, Eq. (A.17) has more than one solution, so that at the same location more than one saturation is obtained, a physical impossibility. a physically impossible solution, because we find that more than one saturation will exist at a single location. This dilemma is resolved by the propagation of discontinuities known as shocks.

There are two shocks in this case. When both dissolution of CO_2 in brine and vaporization of brine into CO_2 are considered, two single-phase regions can be developed: a single-phase gaseous phase region behind the trailing shock and a single-phase aqueous region ahead of the leading shock. Each of these single-phase regions is connected to the two-phase region by a shock.

In the following, the shock which connects the single-phase gaseous phase region to the two-phase region is referred to as the trailing shock. The shock that connects the two-phase region to the single-phase aqueous region is called the leading shock, as it is always ahead of the trailing shock. The approach below is used to locate the shocks.

Consider the trailing shock from the injection (upstream) composition, $G^d_{CO_2}$, to the downstream composition, $G^c_{CO_2}$, in the two-phase region. The material balance equation on the trailing shock gives:

$$\frac{H^d_{CO_2} - H^c_{CO_2}}{G^d_{CO_2} - G^c_{CO_2}} = \frac{H^d_{Brine} - H^c_{Brine}}{G^d_{Brine} - G^c_{Brine}} \tag{A.20}$$

For convenience, and noting that $q^d_D = 1$ since the flow rate upstream of the trailing shock equals the injection rate, we re-write Eq. (A.20):

$$\frac{\alpha^d_{CO_2} - q^c_D\alpha^c_{CO_2}}{G^d_{CO_2} - G^c_{CO_2}} = \frac{\alpha^d_{Brine} - q^c_D\alpha^c_{Brine}}{G^d_{Brine} - G^c_{Brine}} \tag{A.21}$$

where : $H_{CO_2} = q_D\alpha_{CO_2}$

$$= q_D(\rho_{aD}\omega_{CO_2,a}(1 - f_g) + \rho_{gD}\omega_{CO_2,g}f_g) \tag{A.22a}$$

$$H_{Brine} = q_D\alpha_{Brine}$$

$$= q_D(\rho_{aD}\omega_{Brine,a}(1 - f_g) + \rho_{gD}\omega_{water,g}f_g) \tag{A.22b}$$

Solving for q^c_D gives:

$$q^c_D = \frac{\alpha^d_{Brine}(G^d_{CO_2} - G^c_{CO_2}) - \alpha^d_{CO_2}(G^d_{Brine} - G^c_{Brine})}{\alpha^c_{Brine}(G^d_{CO_2} - G^c_{CO_2}) - \alpha^c_{CO_2}(G^d_{Brine} - G^c_{Brine})} \tag{A.23}$$

$G^d_{CO_2}$ and G^d_{Brine} are known and $G^c_{CO_2}$ and G^c_{Brine} are functions of S^c_g only. Application of the entropy condition and velocity constraint (Helfferich, 1982; Lax, 1957) shows that the trailing shock is a semi-shock that satisfies:

$$q^c_D\frac{df_g}{dS_g} = \frac{\alpha^d_{CO_2} - q^c_D\alpha^c_{CO_2}}{G^d_{CO_2} - G^c_{CO_2}} \tag{A.24}$$

Eqs. (A.23) and (A.24) can be solved simultaneously to obtain q^c_D and S^c_g.

The material balance equation on the leading shock gives:

$$\frac{H^a_{CO_2} - H^b_{CO_2}}{G^a_{CO_2} - G^b_{CO_2}} = \frac{H^a_{Brine} - H^b_{Brine}}{G^a_{Brine} - G^b_{Brine}} \tag{A.25}$$

Using Eqs. (A.22a) and (A.22b), this equation becomes:

$$\frac{q^a_D\alpha^a_{CO_2} - q^b_D\alpha^b_{CO_2}}{G^a_{CO_2} - G^b_{CO_2}} = \frac{q^a_D\alpha^a_{Brine} - q^b_D\alpha^b_{Brine}}{G^a_{Brine} - G^b_{Brine}} \tag{A.26}$$

Then:

$$\frac{q^a_D}{q^b_D} = \frac{\alpha^b_{CO_2}(G^a_{Brine} - G^b_{Brine}) - \alpha^b_{Brine}(G^a_{CO_2} - G^b_{CO_2})}{\alpha^a_{CO_2}(G^a_{Brine} - G^b_{Brine}) - \alpha^a_{Brine}(G^a_{CO_2} - G^b_{CO_2})} \tag{A.27}$$

Note that $q^b_D = q^c_D$, since the flow velocity is constant in the two-phase region (q^c_D is already obtained from the solution for the trailing shock). We need one more equation to evaluate q^a_D. This equation is given based on the semi-shock equation:

$$q^b_D\frac{df_g}{dS_g} = \frac{q^a_D\alpha^a_{CO_2} - q^b_D\alpha^b_{CO_2}}{G^a_{CO_2} - G^b_{CO_2}} \tag{A.28}$$

Eqs. (A.27) and (A.28) can be solved simultaneously to obtain q^a_D and S^b_g.

It should be noted that the absolute permeability of the reservoir has no effect on the positions of the shocks and therefore on the

advancement of CO_2 in the reservoir. Absolute permeability only affects the injectivity.

The above formulation in placement of the trailing shock can be obtained graphically: a tangent line from point d on the $H_{CO_2} - G_{CO_2}$ curve gives the trailing shock specifications, whilst a tangent line from point a on the $H_{CO_2} - G_{CO_2}$ curve gives the leading shock specifications. For the case of pure CO_2 injection in a saline aquifer that initially contains brine only, we can write:

$$(G^{d}_{CO_2}, H^{d}_{CO_2}) = (1,1) \quad \text{and} \quad (G^{a}_{CO_2}, H^{a}_{CO_2}) = (0,0) \tag{A.29}$$

This result means that the trailing and leading shocks can be obtained by drawing tangent lines from the origin and point (1, 1) on the $H_{CO_2} - G_{CO_2}$ curve, respectively. The slope of the tangent line gives the similarity variable and the tangent point gives the saturation/concentration at the shock. However, as the $H_{CO_2} - G_{CO_2}$ curve is not pre-determined (it depends on the compositional properties and local flow rate), the above graphical method is impractical. In the following, this graphical method is relaxed to enable placement of the shocks based on the f_g–S_g curve.

For the above case of pure CO_2 injection in a saline aquifer that initially contains brine only, we can also write:

$$\alpha^{d}_{CO_2} = 1,\ G^{d}_{CO_2} = 1,\ \alpha^{d}_{Brine} = 0,\ G^{d}_{Brine} = 0,\ \alpha^{a}_{CO_2} = 0,\ G^{a}_{CO_2} = 0,\ \alpha^{a}_{Brine} = \rho_{Brine}/\rho_{CO_2},\ G^{a}_{Brine} = \rho_{Brine}\rho_{CO_2} \tag{A.30}$$

Combining Eqs. (A.24) and (A.21) using the above expressions gives the following at the trailing shock:

$$\left.\frac{df_g}{dS_g}\right|^{c} = \frac{\alpha^{c}_{Brine}}{G^{c}_{Brine}} \tag{A.31}$$

That gives:

$$\left.\frac{df_g}{dS_g}\right|^{c} = \frac{(\rho_{gD}\omega_{Brine,g} - \rho_{aD}\omega_{Brine,a})f^{c}_{g} + \rho_{aD}\omega_{Brine,a}}{(\rho_{gD}\omega_{Brine,g} - \rho_{aD}\omega_{Brine,a})S^{c}_{g} + \rho_{aD}\omega_{Brine,a}} = \frac{f^{c}_{g} - (\rho_{aD}\omega_{Brine,a}/(\rho_{aD}\omega_{Brine,a} - \rho_{gD}\omega_{Brine,g}))}{S^{c}_{g} - (\rho_{aD}\omega_{Brine,a}/(\rho_{aD}\omega_{Brine,a} - \rho_{gD}\omega_{Brine,g}))} \tag{A.32}$$

or:

$$\left.\frac{df_g}{dS_g}\right|^{c} = \frac{f^{c}_{g} - f^{I}_{g}}{S^{c}_{g} - S^{I}_{g}} \quad \text{where}: (S^{I}_{g}, f^{I}_{g}) = \left(\frac{\rho_{aD}\omega_{Brine,a}}{\rho_{aD}\omega_{Brine,a} - \rho_{gD}\omega_{Brine,g}}, \frac{\rho_{aD}\omega_{Brine,a}}{\rho_{aD}\omega_{Brine,a} - \rho_{gD}\omega_{Brine,g}}\right) \tag{A.33}$$

In other words, the trailing shock saturation can be obtained by drawing a tangent line from point J on the f_g–S_g curve. The obtained saturation can be used along with Eq. (A.21) to determine q^{c}_{D}. This will lead to the following:

$$q^{c}_{D} = \frac{(\rho_{aD}\omega_{CO_2,a} - \rho_{gD}\omega_{CO_2,g})S^{c}_{g} - \Delta\rho_{D}S^{c}_{g} + \omega_{Brine,a}\rho_{aD}}{(\rho_{aD}\omega_{CO_2,a} - \rho_{gD}\omega_{CO_2,g})f^{c}_{g} - \Delta\rho_{D}f^{c}_{g} + \omega_{Brine,a}\rho_{aD} + \rho_{aD}\rho_{gD}\Delta\omega_{CO_2}(S^{c}_{g} - f^{c}_{g})} \tag{A.34}$$

where: $\Delta\rho_D = \rho_{aD} - \rho_{gD}$ and $\Delta\omega_{CO_2} = \omega_{CO_2,a} - \omega_{CO_2,g}$.

Then, the similarity variable of the trailing shock will be obtained by Eq. (A.17). It should be noted that point J on f_g–S_g graph corresponds to point $(G_{CO_2}, H_{CO_2}) = (1,1)$ on the $H_{CO_2} - G_{CO_2}$ graph. Likewise, point I could be determined on the f_g–S_g graph that correspond to $(G_{CO_2}, H_{CO_2}) = (0,0)$ on the $H_{CO_2} - G_{CO_2}$ graph to be used to obtain the saturation of the leading shock. For this purpose, Eq. (A.26) is simplified to the following based on Eq. (A.28):

$$\left.\frac{df_g}{dS_g}\right|^{b} = \frac{\alpha^{b}_{CO_2}}{G^{b}_{CO_2}} \tag{A.35}$$

That can be re-written as:

$$\left.\frac{df_g}{dS_g}\right|^{b} = \frac{f^{b}_{g} - f^{I}_{g}}{S^{b}_{g} - S^{I}_{g}} \quad \text{where}: (S^{I}_{g}, f^{I}_{g}) = \left(\frac{\rho_{aD}\omega_{CO_2,a}}{\rho_{aD}\omega_{CO_2,a} - \rho_{gD}\omega_{CO_2,g}}, \frac{\rho_{aD}\omega_{CO_2,a}}{\rho_{aD}\omega_{CO_2,a} - \rho_{gD}\omega_{CO_2,g}}\right) \tag{A.36}$$

This means that a tangent line drawn from point I on the f_g–S_g curve gives the saturation upstream of the leading shock (S^{b}_{g}). Again, the similarity variable of this shock will be given based on Eq. (A.17).

It can be shown that, if the volume change upon mixing is neglected, points I and J given above will be reduced to the formulation given by Noh et al. (2007).

Appendix B. Procedure for obtaining the solution profile

(1) Plot gaseous phase fractional flow versus gaseous phase saturation (f_g–S_g) curve using Eq. (3). For this purpose, gaseous and aqueous phases viscosities are required, which are obtained using the PVT model at the aquifer conditions.
(2) Obtain the coordinate of point I based on Eq. (11). Draw a tangent line from this point on the f_g–S_g curve. The tangent point is the saturation upstream of the leading shock.
(3) Obtain the coordinate of point J based on Eq. (12). The tangent point obtained by drawing a tangent line from this point on the f_g–S_g curve gives the saturation downstream of the trailing shock.
(4) Obtain the local flow rate in the equilibrium region (q^{c}_{D}) using Eq. (13).
(5) Obtain the similarity variable at the shocks and the saturations in between using Eq. (5).
(6) Obtain the solid salt saturation for the dry-out region using Eq. (14).

Appendix C. Salt precipitation in the dry-out zone

In the following, we develop an equation to calculate the saturation of solid salt in the dry-out zone. From the saturation of gaseous and aqueous phases we can write:

$$\frac{(m_{water,a} + m_{salt} + m_{CO_2,a})/\rho_a}{(m_{CO_2,g} + m_{water,g})/\rho_g} = \frac{1 - S^{c}_{g}}{S^{c}_{g}} \tag{C.1}$$

The molar salt concentration in the aqueous phase is:

$$\frac{m_{salt}}{m_{water,a} + m_{salt} + m_{CO_2,a}} = \omega_{salt,a} \tag{C.2}$$

The mole fraction of CO_2 in aqueous and gaseous phases gives:

$$\frac{m_{CO_2,a}}{m_{water,a} + m_{CO_2,a} + m_{salt}} = \omega_{CO_2,a} \tag{C.3}$$

$$\frac{m_{CO_2,g}}{m_{water,g} + m_{CO_2,g}} = \omega_{CO_2,g} \tag{C.4}$$

The solid salt saturation is defined as:

$$S_{\text{salt}} = \frac{m_{\text{salt}}/\rho_{\text{salt}}}{V} = \frac{m_{\text{salt}}/\rho_{\text{salt}}}{(m_{\text{CO}_2,\text{g}} + m_{\text{water,g}})/\rho_{\text{g}} S_{\text{g}}^{\text{c}}} \tag{C.5}$$

Combining the above equations and solving for solid salt saturation (S_{salt}) gives:

$$S_{\text{salt}} = \frac{\rho_{\text{a}} \omega_{\text{salt,a}}}{\rho_{\text{salt}}} (1 - S_{\text{g}}^{\text{c}}) \tag{C.6}$$

Note that in practice the salinity is given which is defined as:

$$\frac{m_{\text{salt}}}{m_{\text{water,g}} + m_{\text{water,a}} + m_{\text{salt}}} = s \tag{C.7}$$

Combining Eq. (C.7) with Eqs. (C.1)–(C.5), one can calculate the salt concentration in the aqueous phase based on the salinity:

$$\omega_{\text{salt,a}} = s\left(1 - \omega_{\text{CO}_2,\text{a}} + \frac{\omega_{\text{water,g}} S_{\text{g}}^{\text{c}} \rho_{\text{g}}}{(1 - S_{\text{g}}^{\text{c}})\rho_{\text{a}}}\right) \tag{C.8}$$

The latter term in the bracket above can be neglected due to small values of vaporized water in the gaseous phase, therefore:

$$\omega_{\text{salt,a}} = s(1 - \omega_{\text{CO}_2,\text{a}}) \tag{C.9}$$

References

Bolton, E.W., Lasaga, A.C., Rye, D.M., 1999. Long-term flow/chemistry feedback in a porous medium with heterogeneous permeability: kinetic control of dissolution and precipitation. Am. J. Sci. 299, 1–68.

Bruining, J., 2001. Handout of Multiphase Flow in Porous Media. Delft University of Technology.

Buckley, S.E., Leverett, M.C., 1942. Mechanism of fluid displacement in sands. Trans. AIME 146, 187–196.

Burton, M., Kumar, N., Bryant, S.L., 2008. Time-dependent injectivity during CO_2 storage in aquifers. In: SPE/DOE Improved Oil Recovery Symposium, Tulsa, OK.

Dumore, J.M., Hagoort, J., Risseeuw, A.S., 1984. An analytical model for one-dimensional three-component condensing and vaporizing gas drives. Soc. Pet. Eng. J. 24, 169–179.

Fayers, F.J., Sheldon, J.W., 1959. The effect of capillary pressure and gravity on two-phase fluid flow in a porous medium. Trans. AIME 216, 147–155.

Fuller, R.C., Prevost, J.H., Piri, M., 2006. Three-phase equilibrium and partitioning calculations for CO_2 sequestration in saline aquifers. J. Geophys. Res. 111, B06207.

Hassanzadeh, H., Pooladi-Darvish, M., Elsharkawy, A.M., Keith, D.W., Leonenko, Y., 2008. Predicting PVT data for CO_2–brine mixtures for black-oil simulation of CO_2 geological storage. Int. J. Greenhouse Gas Control 2 (1), 65–77.

Hawkins Jr., M.F., 1956. A note on the skin effect, Tech. Note 389. Trans. AIME 207, 356–357.

Helfferich, F.G., 1982. Generalized welge construction for two-phase flow in porous media in system with limited miscibility, SPE 9730. In: SPE Annual Technical Conference and Exhibition, New Orleans, LA.

Hurter, S., Labergere, D., Berge, J., 2008. Simulation for CO_2 injection projects with compositional simulator. In: SPE 108540, Offshore Europe, Aberdeen, Scotland, U.K..

Kleinitz, W., Koehler, M., Dietzsch, G., 2001. The precipitation of salt in gas producing wells SPE 68953. In: SPE European Formation Damage Conference, The Hague, The Netherlands.

LaForce, T., Johns, R.T., 2005. Composition routes for three-phase partially miscible flow in ternary systems. Soc. Pet. Eng. J. 10, 161–174.

LaForce, T., Cinar, Y., Johns, R.T., Orr Jr., F.M., 2006. Experimental confirmation for analytical composition routes in three-phase partially miscible flow. In: SPE/DOE Improved Oil Recovery Symposium, Tulsa, OK.

Lax, P.D., 1957. Hyperbolic conservation laws II. Commun. Pure Appl. Math. 10, 537–566.

Muller, N., Ran, Q., Elizabeth, M., Pruess, K., Blunt, M.J., 2008. CO_2 injection impairment due to halite precipitation. In: 9th International Conference on Greenhouse Gas Control Technologies, Washington, DC, USA.

Nelson, P.H., 1994. Permeability–porosity relationships in sedimentary rocks. Log Analyst 35 (3), 38–62.

Noh, M., Lake, L.W., Bryant, S.L., Araque-Martinez, A., 2007. Implications of coupling fractional flow and geochemistry for CO_2 injection in aquifers. SPE Reservoir Eval. Eng. 10 (4), 406–414.

Orr Jr., F.M., 2007. Theory of Gas Injection Processes. Tie-Line Publications, Copenhagen, Denmark.

Prévost, J.H., Fuller, R.C., Altevogt, A.S., Bruant, R., Scherer, G.W., 2004. Numerical modeling of carbon dioxide injection and transport in deep saline aquifers. In: Proceedings, 7th International Conference on Greenhouse Gas Control Technologies, Vancouver, BC, vol. II (2), Poster Papers. Elsevier Ltd., pp. 2189–2193.

Pruess, K., Muller, N., 2009. Formation dry-out from CO_2 injection into saline aquifers: 1. Effects of solids precipitation and their mitigation. Water Resour. Res. 45, W03402, doi:10.1029/2008WR007101.

Pruess, K., 2009. Formation dry-out from CO_2 injection into saline aquifers: 2. Analytical model for salt precipitation. Water Resour. Res. 45, W03403, doi:10.1029/2008WR007102.

Pruess, K., Spycher, N., 2007. ECO2N—a fluid property module for the TOUGH2 code for studies of CO_2 storage in saline aquifers. Energy Convers. Manage. 48 (6), 1761–1767.

Pruess, K., García, J., Kovscek, T., Oldenburg, C., Rutqvist, J., Steefel, C., Xu, T., 2002. Intercomparison of Numerical Simulation Codes for Geologic Disposal of CO_2, Lawrence Berkeley National Laboratory Report LBNL-51813, Berkeley, CA.

Spycher, N., Pruess, K., 2005. CO_2–H_2O mixtures in the geological sequestration of CO_2. II. Partitioning in chloride brines at 12–100 °C and up to 600 bar. Geochim. Cosmochim. Acta 69 (13), 3309–3320.